Materials and Methods

Neurons cell culture. Primary rat hippocampus neurons (Life Technologies, Carlsbad, CA, USA) were recovered from cryopreservation and seeded on poly-L-lysine (Trevigen, Gaithersburg, MD, USA) coated gold film with a coverage of ~10^5 neurons/cm^2. After incubation in a humidified atmosphere with 5% CO_2 at 37°C for 4~8 days, the neurons attached to the surface and were ready for experiment. The neurons were cultured in neurobasal medium (Life Technologies, Carlsbad, CA, USA) with B-27® supplement (Life Technologies, Carlsbad, CA, USA) and GlutaMAX™ (Life Technologies, Carlsbad, CA, USA).

P-EIM set-up. The plasmonic imaging system was built on an inverted microscope (Olympus IX81) with a total internal reflection fluorescence (TIRF) imaging attachment using a 60× NA 1.49 oil immersion objective. The light source was a 670 nm superluminescent light emitting diode (SLD-26-HP, Superlum, https://www.superlumdiodes.com). For high temporal resolution imaging, an ultra-fast CMOS (Complementary metal-oxide-semiconductor) camera (Phantom V310, Vision Research, http://www.visionresearch.com) with 100,000 frames per second in 256 pixels by 256 pixels was used. For resolving individual action potentials, a low noise sCMOS camera (scientific CMOS, ORCA-Flash 4.0, Hamamatsu, Japan) was used at a frame rate of 1603 fps with 2048 pixels by 128 pixels. Images were directly streamed into a fast solid state drive array with four Samsung 840 pro solid state drives configured in RAID mode 0. To synchronize the electrical recording with plasmonic recording, cameras were externally triggered by the patch clamp voltage controller. The setup was placed on a floating optical table and enclosed in a custom build faradic cage and acoustic enclosure to minimize electrical and mechanical noises. The gold films

were prepared by evaporating 2 nm chromium as adhesion layer, followed by ~47 nm gold layer on BK-7 glass coverslips. Each gold film was washed with water and ethanol followed by hydrogen-flame annealing to remove possible surface contamination. The gold films were modified with 140 µl of 5 µg/ml poly-L-lysine solution in 37 °C for one hour, and further rinsed with deionized water twice prior to cell seeding. A removable Flexi-Perm silicone chamber (SARSTEDT, http://www.sarstedt.com) was placed on top of the gold chip to serve as a culture chamber.

Electrophysiology. Cultured hippocampal neurons were recorded in whole-cell configuration, using Axopatch 200A amplifier (Axon Instruments) at room temperature on the plasmonic imaging set-up. To trigger action potential, depolarizing current pulses with amplitude of 500 pA and duration of 2-4 ms were applied in a current clamp mode. Glass micropipettes were prepared by a flaming puller (P-97, Sutter Instrument, CA), which were filled with 10 mM NaCl, 135 mM K-gluconate, 10 mM HEPES, 2 mM $MgCl_2$, 2 mM Mg-ATP and 1 mM EGTA (pH 7.4). The resistance of these micropipettes is 5-10 MΩ. The extracellular recording solution contains 135 mM NaCl, 5 mM KCl, 1.2 mM $MgCl_2$, 5 mM HEPES, 2.5 mM $CaCl_2$ and 10 mM glucose at pH 7.4.

Ion channel inhibitors TTX (1 µM) was added to the above extracellular recording solution for control experiments. For cytochalasin D (CD) treatment, the stock solution was diluted with culture medium to a final concentration of 10 mM, and the neurons were incubated at 37 °C for 30 min in the CD-containing media before measurements. Control neurons were maintained in the normal culture media. Experiments with and without CD-treated neurons were performed in the normal recording media.

Data analysis. Raw plasmonic images were spatially smoothed with 11×11 pixel (3.3×3.3 μm) mean kernel. The mean image stack was obtained by averaging over multiple cycles with cycle number between 40-150 (Supplementary Information, section 2). Local response profiles were plotted as traces of image intensity changes at selected regions of interest (ROIs) in the cycle-averaged image stack. Optical response was examined and displayed in a differential way by subtracting the first image of the mean image stack. To remove spatial noises, the mean image stack was temporally detrended pixel by pixel using a fitted linear function. High frequency noise was further suppressed by a digital finite impulse response low-pass filter with 1 kHz cut-off frequency. For individual spike resolving, a 50 ms moving average signal of intensity profile from the ROI was removed to subtract out the long-term drift (20 Hz high-pass filter). Bands at frequencies of 60 Hz, 120 Hz, 180 Hz, 300 Hz, 420 Hz and 540 Hz were digitally filtered, which were typical noise from electrical sources. Intensity profile was further smoothed with 5 ms moving average for plotting. The electrical signals recorded with the patch clamp were filtered by a 2 kHz low-pass Bessel filter. To accurately identify the time-lag of action potential propagation, Lorentzian function was utilized to fit the peak position of action potential at different region. All post-acquisition analyses were carried out by custom-written MATLAB (Natick, MA, USA) codes.

Supporting Text

1. Observation of failed action potential firing

We observed that in some cycles action potentials failed to fire in the plasmonic recording. This phenomenon is common in the traditional patch-clamp electrical recording of action potential. This characteristic is distinctly different from the passive depolarization and polarization of the membrane, which are always accompanied with electrical triggering (Figure S2).

2. Quantification of the noise level

We quantified the neuronal plamonic response for action potential. In consistence with the electrical modulation results, 100 mV potential depolarization during action potential also gives about 0.3-1‰ baseline intensity change (Figure S4a). The standard deviation of raw plasmonic intensity for the whole cell in our current system is about 0.3‰ (Figure S4a), which is at the similar level to the signal. After cycle averaging, system noise was greatly suppressed. Ten cycles averaged provided a signal-to-noise ratio around 3, which was sufficient to see the plasmonic peak induced from action potential (Figure S4a). Typically, we used 40-150 stimulation cycles averaging to get clear imaging data for action potential firing, with typical signal-to-noise ratio about 5-10 (Figure S4b). We plotted the standard deviation of plasmonic intensity with averaging cycles. The noise level decreases following a power-law form, with power coefficient of ~ 0.5, which indicates that the system is shot noise limited.

3. P-EIM system calibration

a) Calibration of plasmonic image intensity versus ionic concentration

To study the relative plasmonic image intensity in buffer with different ionic strength, we calibrated the plasmonic image intensity change in 0.8×, 0.85×, 0.9×, 0.95× and 0.975× Phosphate-buffered saline (PBS) solutions in respect to 1× PBS (Figure S5). The ionic strength of 1× PBS is ~160 mM. We plotted the decrease of ionic strength with the intensity change in the plasmonic images. A linear relationship was observed. The fitted coefficient was ~$2 \times 10^{-3}\ \Delta I/I \cdot mM^{-1}$. Since refractive index change from 1× PBS to 0.9× PBS (16 mM concentration difference) typically gives 23 mDeg angular shift in surface plasmonic resonance angle,[1] the calibration factor for angular shift is about $1.3\ \Delta I/I \cdot Deg^{-1}$. According to this calibration, the observed plasmonic signal at the action potential peak is about ~0.2 mDeg.

b) Calibration of plasmonic image intensity versus applied surface potential

To calibrate the plasmonic image intensity versus the surface potential, we applied potential steps (from -100 mV to 150 mV with 50 mV steps) onto the P-EIM sensor chip, referencing to the counter electrode in the 1× PBS solution. The sensor chip was pre-coated with poly-L-lysine using the same protocol as in the neuron culture case. The plasmonic intensity has the same sign with the applied potential (Figure S6). With small potential applied onto the surface, a quasi-linear relationship was observed. A typical number for the surface capacitance of modified gold surface in PBS is about 5 μF/cm^2.[2] Therefore, from -50 mV to +50 mV, a total 100 mV surface potential change gives surface charge density ($\Delta\sigma$) of $5\ \mu F/cm^2 \times 100\ mV\ = 5 \times 10^{-3}\ C/m^2$. From the calibration curve, this 100 mV signal induces $3.7 \times 10^{-3}\Delta I/I$ change, which equal to 2.8 mDeg of angular shift, $\Delta\theta$. Thus we can experimentally calibrate effective α from the relationship $\Delta\sigma = \alpha\Delta\theta$, which is ~$2\ C \cdot m^{-2} \cdot Deg^{-1}$. This number is ~10 times smaller than that from the theoretical calculation.[2a] We anticipate the difference comes

from the mechanical amplification effect from the poly-L-lysine layer modified on the surface, which is coupled with the charge change.[3]

4. Contributions to plasmonic imaging intensity

a) Electrical contribution to the P-EIM signal

The local surface charge density ($\Delta\sigma$) and surface plasmon resonance angle change ($\Delta\theta$) are related by $\Delta\sigma = \alpha\Delta\theta$, where α is a constant.[2a] From the calibration curve (Figure S6), α is about 2 $C\cdot m^{-2}\cdot deg^{-1}$. The transient charge change due to the ionic flux during the action potential was estimated by $\Delta\sigma_t = C_m\Delta V_m$, where $\Delta\sigma_t$ is the total charge change per unit area, C_m is the membrane capacitance and ΔV_m is the membrane potential change when action potential fires. Cell membrane has a typical capacitance of ~1 $\mu F/cm^2$. Depolarization phase of the action potential gives ~100 mV membrane potential change. Therefore, the total charge flux during action potential depolarization phase is estimated to be 10^{-3} C/m^2. If all these charges contribute to the charge density change on the surface, the estimated plasmonic signal (θ) will be ~0.5 mDeg, which is in the same order of observed signal but several times higher (~0.2 mDeg for observation). Given that this estimation likely overestimates the real charge induced on the gold surface, this calculation is reasonable comparing with the experimental observation. The observed negative plasmonic responses indicate negative charges on the surface, which is in consistence with the theoretical model that the inward sodium current causes depletion of positive charges outside of the cell and forms a sink region when cell depolarized. P-EIM measures the total charge. The shape of the plasmonic response should resemble the integration of ionic current, as well as the capacitive membrane potential. This observation agrees to the presumption.

b) Electromechanical contribution to the P-EIM signal

The coupling effect between electrical and mechanical signals may also indirectly contribute to the impedance response that measured by P-EIM. The electromechanical coupling phenomenon has been observed using various probing and optical methods[4]. Most of these studies were conducted on nerve fibers or cancer cell lines. The detected signals were typically in nanometer to sub-nanometer range. Since the complexity of the biological system and extreme small signals involved, various mechanisms have been proposed, such as thermodynamic model,[4e] channel tension model,[5] lipid orientation model,[6] soliton model[7] and ion hydration model.[4c] Although many complications are involved in explaining the phenomenon, all these studies indicate that the electromechanical coupling may contribute to the impedance signal we detected.

The plasmonic wave decays from the surface to the solution with typical decay length ~100 nm.[8] If we assume that the observed impedance signal fully comes from the mechanical deformation, the maximum displacement at the action potential peak is estimated to be ~0.05 nm to the direction that moves away from the surface. This number is smaller than what has been reported on mammalian cell lines using AFM. The displacement direction is also opposite to what has been observed. However, P-EIM detects the bottom cell membrane rather than the top membrane. Considering the strains between bottom membrane and sensing surface, structural and mechanical difference between primary neurons and cell lines and configuration difference between P-EIM and AFM for deformation detection, the observed amplitude and direction is possible. To further examine the possible mechanical deformation of the membrane, we measured neurons treated with cytochalasin D, which is known to soften the cell by inhibiting polymerization of the actin, a major component of the cytoskeleton of the cell. We observed a slight increase in the action potential peak by the plasmonic recording in cytochalasin D-treated neurons ($p = 0.27$, t-test) (Figure S7). This

observation indicates that the membrane deformation may partially contribute to the plasmonic signals.

c) Refractive index contribution to the P-EIM signal

Because P-EIM is also sensitive to the refractive index change close to the sensing surface, it is likely that the ion flux during action potential may cause local refractive index change and thus contribute to the plasmonic signal. The total amount of fluxed sodium ion during the action potential can be calculated by $n_{Na^+} = \Delta\sigma_{Na^+}/F$, where $\Delta\sigma_{Na^+}$ is the charge flux of sodium ions, F is Faraday constant and n_{Na^+} is the molar amount of sodium ion flux. According to the estimation above, the total charge flux during depolarization phase is ~10^{-3} C/m^2. Therefore, we calculate the total amount of inward sodium ions is ~10^{-8} mol/m^2 at the membrane areas. Since the diffusion coefficient (D) of Na^+ ions in water at room temperature is 1.33×10^{-5} cm$^2\cdot$s^{-1}, according to the diffusion equation, $l = \sqrt{2Dt}$, the averaged diffusion distance for Na^+ ions is 2.3 μm during the 2 ms action potential excitation period. This number is small comparing with the diameter of the neuron. Therefore, the sodium ion in the junction region between the bottom cell membrane and the sensing surface will be depleted when cell membrane depolarizes. The height of this junction region is typically ~100 nm. We can calculate the sodium ion concentration decrease in this region by dividing the total sodium ion flux with the volume in this region, which is ~0.1 mM. According to calibration curve, ~0.1mM extracellular concentration (PBS) change corresponds to a shift in plasmonic signal of 0.14 mDeg. Suppose that the refractive index change is mainly from the salt sodium chloride, we can simply estimate the contribution from sodium ion itself by Lorentz-Lorenz equation:

$$\frac{n^2-1}{n^2+2} = \sum_i \frac{4\pi\alpha_i N_i}{3}$$

where n is refractive index, α_i is the polarizability (in volume) of the ith molecule and N_i is the number density of the ith molecule. With the same molar concentration of Na^+ and Cl^-, the small increase in refractive index (Δn), comparing with pure water n_w, is proportional to the polarizability of these two ions adding to the water. However, the polarizability of chloride ion is at least 20 times bigger than the sodium ion.[9] Thus, the depletion of ~0.1 mM sodium ion itself will only give <0.007 mDeg plasmonic shift, which is 30 times smaller than the observed signal. Therefore, we can rule out the contribution from the refractive index change induced by the ionic flux.

Supporting Figures

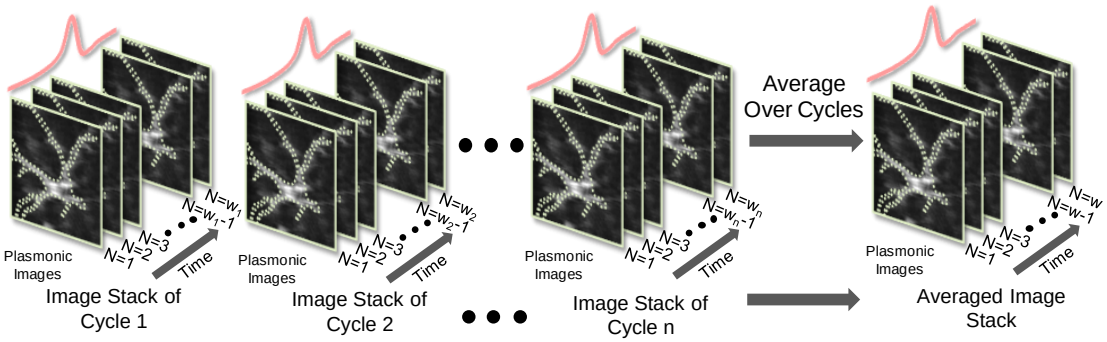

Figure S1. In order to optically resolve the action potential firing in neurons, multiple cycles of stimulation were applied and the plasmonic images recorded among these cycles were averaged to improve the signal-to-noise ratio. Plasmonic responses were imaged with an ultrafast camera at a frame rate of 10,000 fps. Images stacks for each stimulation cycles were then registered and averaged over cycles.

We triggered neuronal action potential repeatedly at a frequency of 50 Hz. In some cycles, action potential was not excited, as shown in the P-EIM images (Figure S2). The failure of action potential excitation during repeated stimulation of neurons is due to the lack of sufficient time for voltage-gated ion channels to recover from the desensitization state [10]. This is a distinct feature of action potential, and does not occur in the passive response of membrane polarization to current injection. The observation of action potential failure in some stimulation cycles thus confirms that the plasmonic image intensity response is due to action potential rather than passive membrane polarization (Figure S2).

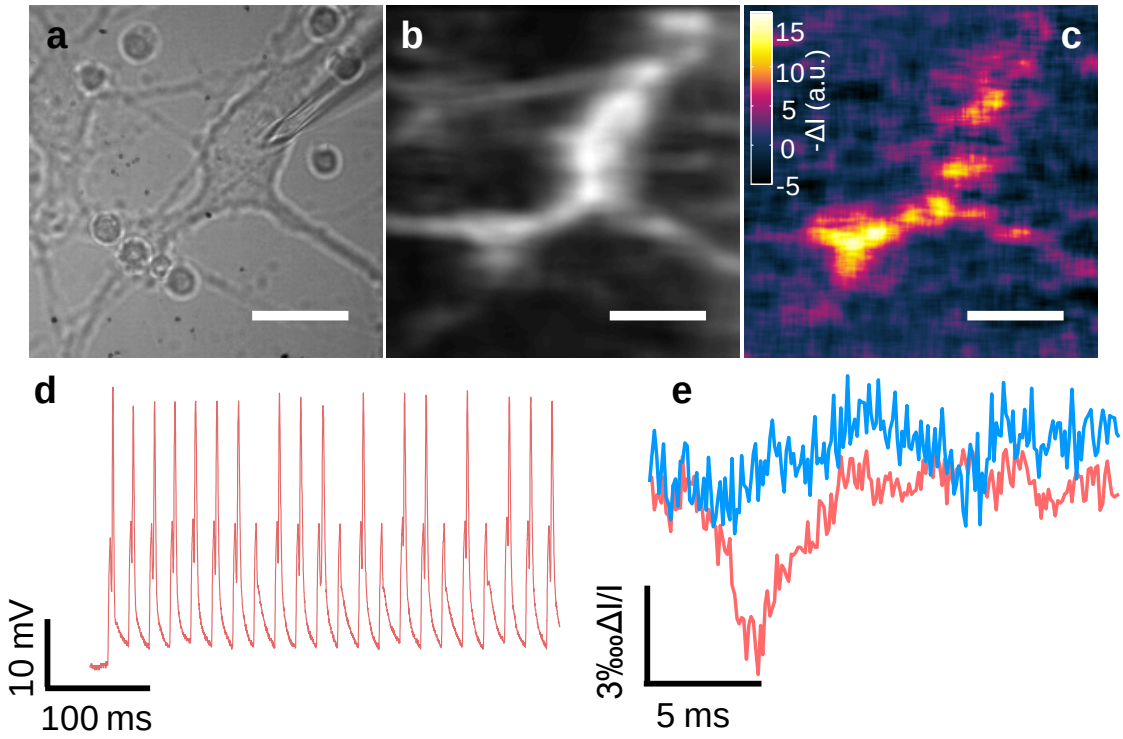

Figure S2. Failed cycles of action potential firing. (a) Optical transmission and (b) plasmonic images of hippocampal neurons. (c) A snapshot plasmonic imaging of action potential at 4 ms after triggering. (d) Electrical recording of action potential with patch clamp. (e) Plasmonic recording of a successful (blue) and failed (red) action potential firing.

To resolve single action potential spikes without averaging over repeated cycles, we suppressed the noise in the images using a low noise sCMOS camera. Figure S3 shows the individual action potential spikes recorded with P-EIM (bottom red plot), and those recorded simultaneously with patch clamp electrode (top blue plot) in a neuron. Despite the remaining noise, the individual action potential spikes are clearly resolved.

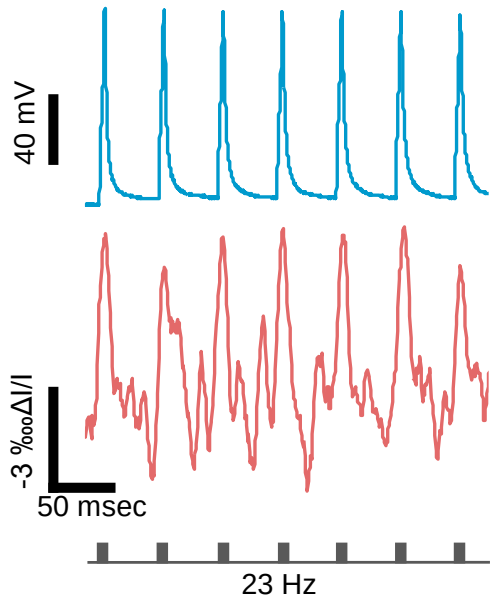

Figure S3. Plasmonic (red) and patch clamp (blue) recordings of individual action potential spikes of a neuron triggered with current pulses at frequency of 23 Hz (plasmonic frame rate: 1,600 fps)

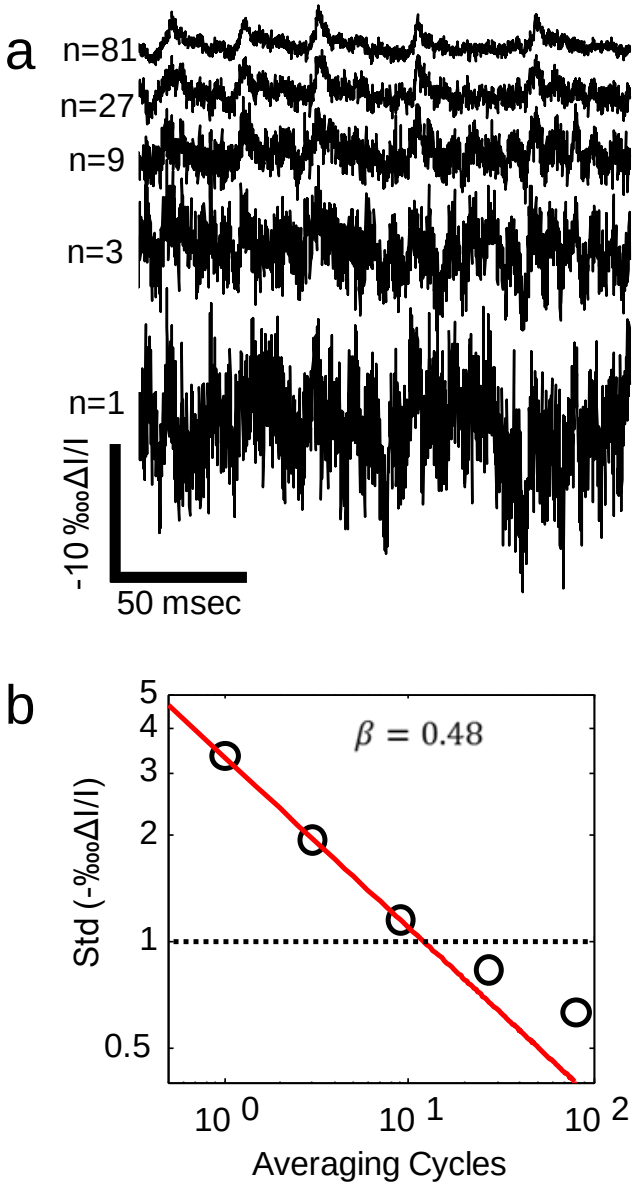

Figure S4.

Figure S4. Plasmonic imaging of single action potential. (a) Different averaged cycles of five action potential spikes. (b) Standard derivation versus the averaged cycles. Data was fitted with linear regression.

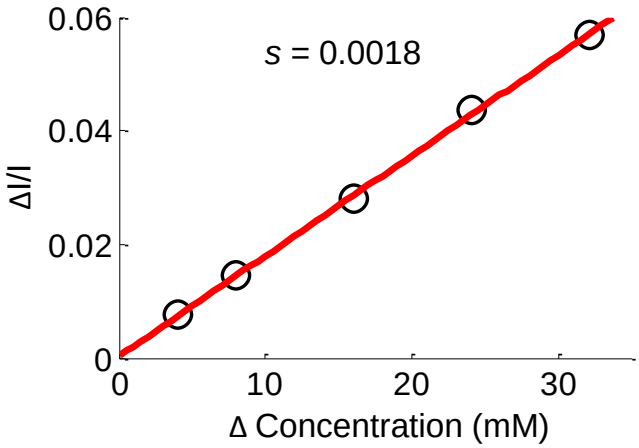

Figure S5. Calibration of plasmonic image intensity versus solution ionic strength with PBS buffer. We measured the plasmonic image intensity change induced by 0.8×, 0.85×, 0.9×, 0.95× and 0.975× PBS solutions in respect to 1× PBS. The ionic strength of 1× PBS is ~160 mM.

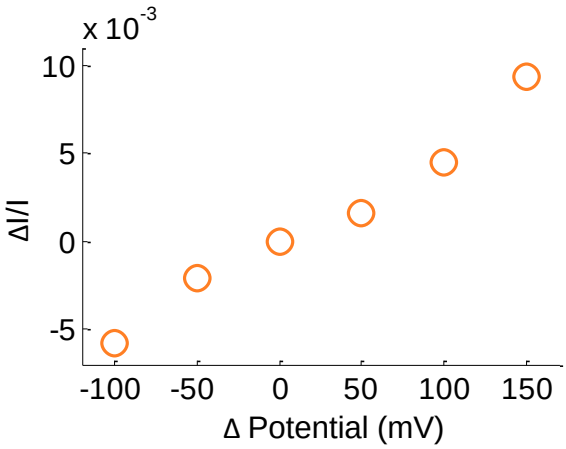

Figure S6. Calibration of plasmonic image intensity response to surface potential. We applied potential steps (from -100 mV to 150 mV with 50 mV steps) onto the P-EIM sensor chip, in reference to the electrode in the 1× PBS solution. By plotting the corresponding plasmonic image intensity changes versus surface potential, a calibration curve is obtained.

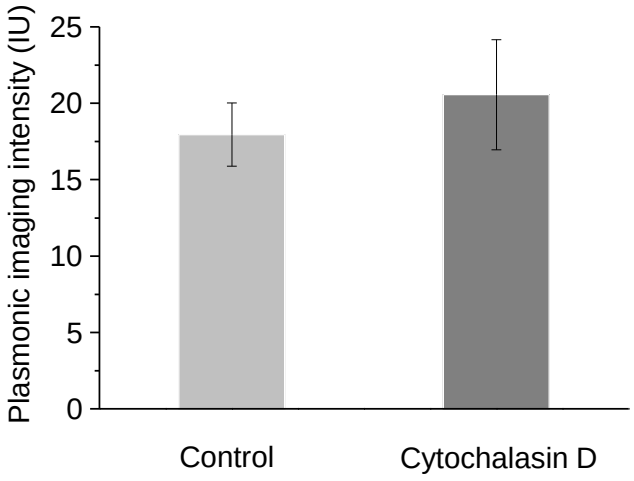

Figure S7. Effect of cytochalasin D, an actin polymerization inhibitor, on the plasmonic signals. Five CD-treated and 10 control neurons were studied.

References

[1] L. Yin, S. Wang, X. Shan, S. Zhang, N. Tao, *Review of Scientific Instruments* **2015**, *86*, 114101.

[2] a) K. J. Foley, X. Shan, N. J. Tao, *Analytical Chemistry* **2008**, *80*, 5146-5151; b) M. D. Porter, T. B. Bright, D. L. Allara, C. E. D. Chidsey, *Journal of the American Chemical Society* **1987**, *109*, 3559-3568.

[3] C. MacGriff, S. Wang, P. Wiktor, W. Wang, X. Shan, N. Tao, *Analytical Chemistry* **2013**, *85*, 6682-6687.

[4] a) T. Akkin, C. Joo, J. F. de Boer, *Biophysical Journal* **2007**, *93*, 1347-1353; b) K. Iwasa, I. Tasaki, R. Gibbons, *Science* **1980**, *210*, 338-339; c) G. Kim, P. Kosterin, A. Obaid, B. Salzberg, *Biophysical Journal* **2007**, *92*, 3122-3129; d) T. D. Nguyen, N. Deshmukh, J. M. Nagarah, T. Kramer, P. K. Purohit, M. J. Berry, M. C. McAlpine, *Nat Nano* **2012**, *7*, 587-593; e) P. C. Zhang, A. M. Keleshian, F. Sachs, *Nature* **2001**, *413*, 428-432.

[5] A. Beyder, F. Sachs, *Proceedings of the National Academy of Sciences* **2009**, *106*, 6626-6631.

[6] R. A. Stepnoski, A. LaPorta, F. Raccuia-Behling, G. E. Blonder, R. E. Slusher, D. Kleinfeld, *Proceedings of the National Academy of Sciences* **1991**, *88*, 9382-9386.

[7] T. Heimburg, A. D. Jackson, *Proceedings of the National Academy of Sciences of the United States of America* **2005**, *102*, 9790-9795.

[8] a) X. Shan, Y. Fang, S. Wang, Y. Guan, H.-Y. Chen, N. Tao, *Nano Letters* **2014**, *14*, 4151-4157; b) X. Shan, S. Wang, N. Tao, *Applied Physics Letters* **2010**, *97*, 223703.

[9] J. J. Molina, S. Lectez, S. Tazi, M. Salanne, J.-F. Dufrêche, J. Roques, E. Simoni, P. A. Madden, P. Turq, *The Journal of Chemical Physics* **2011**, *134*, 014511.

[10] B. P. Bean, *Nat Rev Neurosci* **2007**, *8*, 451-465.

Movie captions

Movie S1 Action potential video imaged at 10,000 frame rate. The movie is averaged over 145 temporally registered action potentials. Movie acquired on a CMOS camera. The Figs. 2e-h in the manuscript are the snapshots from this video.

Movie S2 Action potential video imaged at 100,000 frame rate. The movie is averaged over 68 temporally registered action potentials. Movie acquired on a CMOS camera. The Figure 3e in the manuscript are the snapshots from this video.